CrossMark

ORIGINAL PAPER

Nanoparticles tungstophosphoric acid supported on polyamic acid: catalytic synthesis of 1,8-dioxo-decahydroacridines and bulky bis(1,8-dioxo-decahydroacridine)s

Masoud Nasr-Esfahani[1] · Zahra Rafiee[1] · Hassan Kashi[1]

Abstract Tungstophosphoric acid nanoparticles supported on polyamic acid (TPA NPs/PAA) was prepared and employed as a catalyst for the facile selective synthesis of 1,8-dioxo-decahydroacridines and some bulky bis(1,8-dioxo-decahydroacridine)s via one-pot condensation of 5,5-dimethyl-1,3-cyclohexanedione and various aldehydes with aniline or ammonium acetate in ethanol–water solution. This catalyst was characterized by FT-IR, X-ray diffraction (XRD), field emission scanning electron microscopy (FESEM), transmission electron microscopy (TEM), thermogravimetric analysis (TG), energy-dispersive X-ray analysis (EDAX), and inductively coupled plasma optical emission spectrometry (ICP-OES). The catalyst showed high thermal stability and good reusability. The products were isolated in high purity and the catalyst was easily separated in a simple workup and recycled several times without noticeable loss of activity under the described reaction conditions. The reaction is characterized by short reaction time, high efficiency, and mild reaction conditions.

Keywords Heterogeneous catalyst · Bis(1,8-dioxo-decahydroacridine) · Polyamic acid · Tungstophosphoric acid · Nanoparticle · Supported catalyst

Introduction

Acridine derivatives, especially 1,8-dioxo-decahydroacridine, are an important class of heterocyclic compounds.

✉ Masoud Nasr-Esfahani
manas@yu.ac.ir

[1] Department of Chemistry, Yasouj University, Yasouj 75918-74831, Iran

These compounds are polyfunctionalized 1,4-dihydropyridines. They have a wide range of pharmacological properties, such as antitumor [1], antimalarial [2], antimicrobial [3], and fungicidal [4], and are prescribed as calcium b-blockers [5]. Also, 9-arylacridines interact strongly with topoisomerase-I (Topo-1) and act as anticancer agents [6]. Bucricaine is used topically for surface anesthesia of the eye and given by injection for infiltration anesthesia, peripheral nerve block, and spinal anesthesia. Quinacrine is also known as mepacrine. It acts as a gametocytocide. It destroys the sexual erythrocytic forms of plasmodia and acts as an antimalarial agent. Proflavine is found to be active as bacteriostatic against many Gram-positive bacteria [7]. Amsacrine is an antineoplastic agent. It has been used in acute lymphoblastic leukemia (Scheme 1) [8]. In addition, 1,8-dioxo-decahydroacridines are used as laser dyes [9, 10] and photoinitiators [11].

Multicomponent reactions of aldehydes, ammonium acetate or amines and dimedone are used for the preparation of 1,8-dioxo-decahydroacridines in the presence of various catalysts such as amberlyst-15 [12], ceric ammonium nitrate (CAN) [13], Brønsted acidic imidazolium salts [14], $CeCl_3 \cdot 7H_2O$ [15], 4-dodecylbenzenesulfonic acid (DBSA) [16], 1,3-disulfonic acid imidazolium carboxylate ionic liquids [17], FSG-Hf(NPf$_2$)$_4$ [18], [MIMPS]$_3$PW$_{12}$O$_{40}$ [19], and protic pyridinium ionic liquid ([2-MPyH]OTf) [20].

However, many of these methods suffer from disadvantages such as long reaction times, toxic organic solvents, unsatisfactory yields, and expensive catalysts. Thus, the development of simple, efficient, and high-yielding methods using new catalysts for the synthesis of these compounds would be highly desirable. In recent years, nanocatalysts such as ZnO nanoparticles [21], nano titanium dioxide [22], sulfonic acid-functionalized nanoporous silica
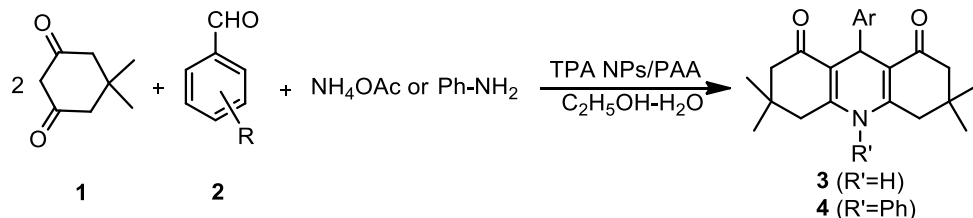
Scheme 1 Representative drugs with acridine constitutional formula

Proflavine   Amsacrine   Quinacrine   Bucricaine
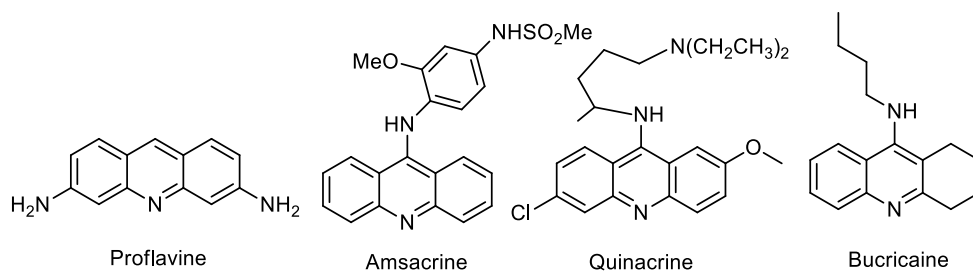
Scheme 2 Synthesis of 1,8-dioxo-decahydroacridines

(SBA-Pr-SO$_3$H) [23], and Fe$_3$O$_4$ nanoparticles [24] have been used for the synthesis of 1,8-dioxo-decahydroacridines. Also the use of Fe$_2$O$_3$@SiO$_2$-PW has been reported for the synthesis of acridines, but no selectivity has been observed [25].

The major drawbacks of heteropoly acids are extreme water solubility, hard recovery, and recycling which limit their practical applications. The utilization of heteropoly acids supported on polymer as heterogeneous catalysts in organic synthesis seems to be one of the most attractive ways to avoid the above-mentioned problems. They are referred to as environmentally benign catalysts because of their non-polluting properties [26]. In general, heteropoly acids supported on polymer offer higher surface area, high atom efficiency, easy product purification, and simple reusability.

In continuation of our interest in the application of heterogeneous catalysts to the development of synthetic methods [27–31], herein we report a simple and highly efficient route for the synthesis of 1,8-dioxo-decahydroacridines using tungstophosphoric acid nanoparticles supported on polyamic acid (TPA/PAA) as a recoverable catalyst with high catalytic activity under reflux conditions in ethanol–water as solvent (Schemes 2, 3).

Experimental

Chemicals were purchased from Merck or Aldrich. IR spectra were recorded from KBr discs on a JASCO FT-IR-680. NMR spectra were taken with a Bruker 400 MHz Ultrashield spectrometer at 400 MHz (^{1}H) and 100 MHz (^{13}C) using CDCl$_3$ or DMSO-d$_6$ as a solvent. Energy-dispersive X-ray spectroscopy analyses (EDAX) were carried out on a PHILIPS XL30, operated at a 20 kV accelerating

voltage. Thermal degradation of polymers was carried out in the range 28–800 °C at a heating rate of 10 °C/min under nitrogen atmosphere using a thermogravimetric analyzer-TG-209 F3, Netzsch, Germany. Optical rotation was obtained with the Jasco p-1030 polarimeter. The morphology of the polymer and catalyst was observed using field emission scanning electron microscopy (FE-SEM) (KYKY-EM-3200) and the X-ray diffraction (XRD) patterns of the polymer and catalyst were recorded using an XRD (Bruker, D8 Advance, Rheinstetten, Germany) with a copper target at 40 kV and 35 mA and Cu Kα ($\lambda = 1.54$ Å) in the range of 10°–80° at the speed of 0.05°/min. Transmission electron microscopy was recorded using a Zeiss-EM10C operated at a 100 kV accelerating voltage. The inductively coupled plasma optical emission spectrometry (ICP-OES) spectra were recorded using an ICP-OES-730-Varian instrument. The melting points were determined using an electrothermal digital melting point apparatus and are uncorrected. Reaction courses and product mixtures were monitored by thin-layer chromatography (TLC).

Synthesis of polymer

To a 50 mL three-necked round-bottomed flask equipped with a high-power electromagnetic stirrer and N$_2$ inlet, 3,5-diamino-1,2,4-triazole (**11**, 0.500 g, 5.05 mmol) and freshly distilled NMP (4 mL) were added. A clear diamine solution was formed after stirring for 5 min. Then, 3,3′,4,4′-benzophenonetetracarboxylic dianhydride (BTDA) **10** (1.100 g, 5.05 mmol) was added immediately, followed by additional NMP (2 mL) to adjust the solid content of the mixture to be 20 wt%. The mixture was stirred at room temperature for 24 h to afford an almost colorless, highly viscous solution. The inherent viscosity of the resulting PAA was 0.75 dl g^{-1}, which was measured in

Scheme 3 Selective synthesis of 1,8-dioxo-decahydroacridines and bis(1,8-dioxo-decahydroacridine)s from dialdehyde, amine, and dimedone with different molar ratios
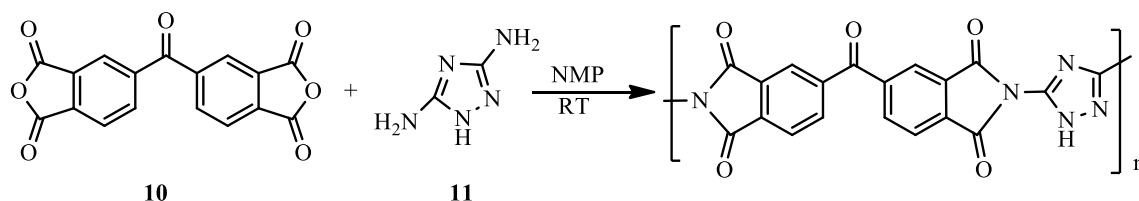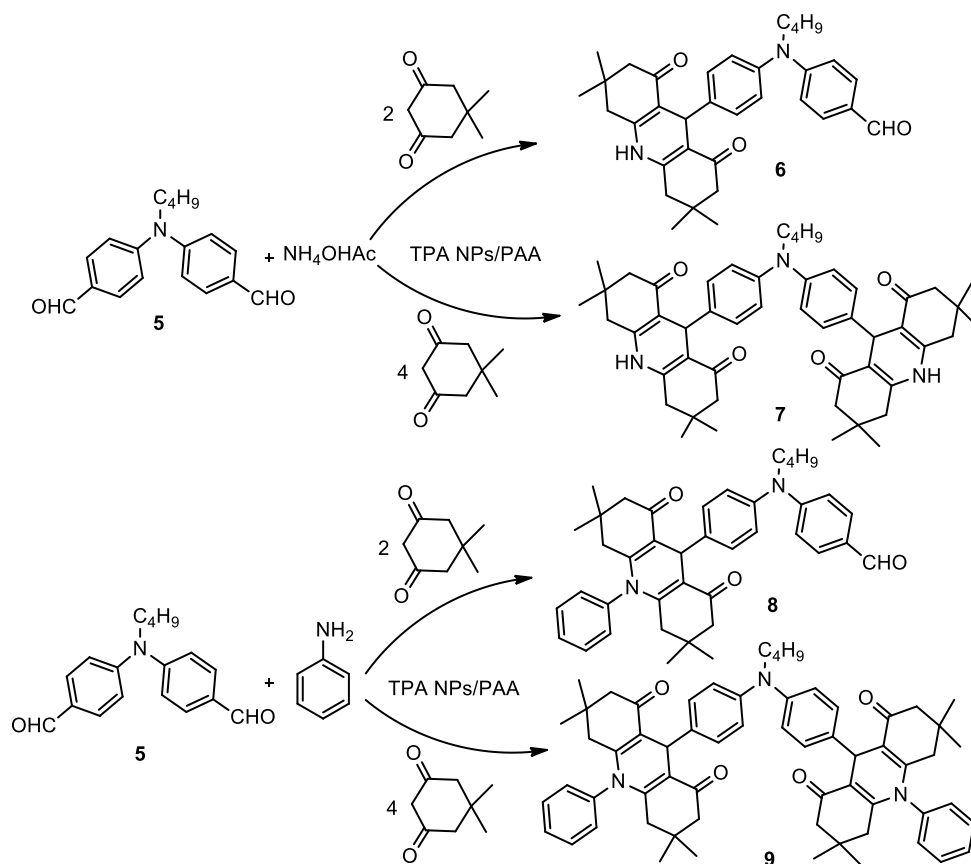
Scheme 4 Synthesis of polyamic acid (PAA)

DMF at a concentration of 0.5 g dl^{-1} at 25 °C (Scheme 4) [32].

$[\alpha]_D^{20} = +38.4°$ ($c = 0.005$ g/mL, DMF); IR (KBr, cm^{-1}): 3490, 3064, 2925, 1785, 1589, 1450, 1346, 1292, 1182, 917, 856, 798.

Preparation of TPA NPs/PAA

Polyamic acid (5 g) in 10 mL of DMF was stirred at 50 °C. Tungstophosphoric acid (1.5 g) was dissolved in deionized water and impregnated dropwise into the mixture and was stirred for 0.5 h at 50 °C and 24 h at room temperature. After evaporating the solvent under reduced pressure, a brown solid was obtained. The solid was washed with distilled water and filtered. This work was repeated until the

pH of effluent water was neutralized. The resulting solid was titrated with sodium hydroxide solution and the supported acid was determined to be 98 %. Thus, with respect to the initial amount of polymer and acid, the catalyst was 30 % w/w from heteropoly acid relative to polyamic acid. IR (KBr, cm^{-1}): 3320, 3064, 2925, 1785, 1727, 1589, 1450, 1346, 1292, 1098, 1065, 980, 836, 634.

Synthesis of *N*-butyl-*N*-phenylaniline

In a round-bottom flask, 1-bromobutane (2.74 g, 0.02 mol), diphenylamine (2.014 g, 0.012 mol), and sodium hydroxide (4.0 g, 0.1005 mol) were added in dimethylsulfoxide (30 mL), followed by heating at 110 °C for 12 h. After cooling to room temperature the resulting mixture was

extracted with ethyl acetate/water. The solvent was evaporated and the resulting crude liquid was purified by column chromatography on neutral alumina using hexane as solvent to give a colorless liquid with a yield of 80.2 %. ^{1}H·NMR (CDCl$_3$), δ (ppm): 7.27–7.23 (4H, m, Ar–H), 6.98–6.96 (4H, m, Ar–H), 6.94–6.92 (2H, m, Ar–H), 3.61 (2H, t, $J = 8.0$ Hz, N–CH$_2$), 1.44–1.42 (2H, m, CH$_2$), 1.31–1.29 (2H, m, CH$_2$), 0.89 (3H, t, $J = 7.0$ Hz, CH$_3$).

Synthesis of 4,4′-(butylazanediyl)dibenzaldehyde (5)

Under N$_2$ atmosphere at 0 °C, freshly distilled POCl$_3$ (23.1 mL, 25 eq.) was added dropwise to DMF (17.6 mL, 23 eq) and then stirred for 1 h. Then, *N*-butyl-*N*-phenylaniline (2.230 g, 9.9 mmol) was added to this solution, and the resulting mixture was stirred for 4 h at 95 °C. After cooling to room temperature, the mixture was poured into a beaker containing ice cubes and basified with 4 M NaOH. The resulting mixture was extracted with EA/brine. After evaporating the organic solvent, the crude product was purified by column chromatography on neutral alumina using a mixture of ethylacetate/*n*-hexane (1:4, v/v), to give a pale green liquid (2.5 g, yield = 90 %). ^{1}H·NMR (CDCl$_3$), δ (ppm): 9.85 (2H, s, CHO), 7.78 (4H, d, $J = 8.4$ Hz, Ar–H), 7.13 (4H, d, $J = 8.4$ Hz, Ar–H), 3.82 (2H, t, $J = 8.0$ Hz, N–CH$_2$), 1.45–1.41 (2H, m, CH$_2$), 1.30–1.26 (2H, m, CH$_2$), 0.85 (3H, t, $J = 6.5$ Hz, CH$_3$).

General procedure for the synthesis of 1,8-dioxo-decahydroacridine

In a 25 mL flask, a mixture of aldehyde (1 mmol), 5,5-dimethyl-1,3-cyclohexanedione (2 mmol), amine (1 mmol) and nanoparticles TPA/PAA (30 wt%, 0.04 g) was refluxed in ethanol–water (2 mL, v/v = 1) for 0.5–1 h. After completion of the reaction as monitored by TLC, because the heterogeneous catalyst was insoluble in ethanol–water, it was removed by filtration and the solution was cooled to room temperature and the pure product was crystallized in EtOH to form crystals. The removed catalyst was washed with ethanol and dried prior to reuse in subsequent reactions.

4-(Butyl(4-(3,3,6,6-tetramethyl-1,8-dioxo-1,2,3,4,5,6,7,8,9,10-decahydroacridin-9-yl)phenyl)amino)benzaldehyde (**6**): Cream solid; mp: 161–163 °C; [α]$_D^{20}$ = +109.2° (c = 0.021 g/mL, CHCl$_3$); IR (KBr, cm^{-1}): 3282, 3066, 2956, 2871, 1683, 1643, 1608, 1484, 1220; ^{1}H·NMR (400 MHz, DMSO-d$_6$) δ (ppm): 9.71 (1H, s, CHO), 8.32 (1H, s, NH), 7.81 (2H, d, $J = 8.1$, Ar–H), 7.08 (2H, d, $J = 8.5$, Ar–H), 6.91 (2H, d, $J = 8.1$ Hz, Ar–H), 6.40 (2H, d, $J = 8.5$ Hz, Ar–H), 4.73 (1H, s, CH), 4.14 (1H, q, $J = 7.2$ Hz, N–CH$_2$), 3.77–3.71 (1H, q, $J = 7.6$ Hz, N–CH$_2$), 2.52 (2H, d, CH$_2$, $J = 18.0$ Hz), 2.45 (2H, d, CH$_2$,

$J = 16.3$ Hz), 2.16 (4H, s, 2×CH$_2$), 1.56–1.48 (2H, m, CH$_2$), 1.34–1.26 (2H, m, CH$_2$), 1.10 (6H, s, 2×CH$_3$), 1.00 (6H, s, 2×CH$_3$), 0.90 (3H, t, $J = 3.5$ Hz); ^{13}C NMR (100 MHz, CDCl$_3$) δ (ppm): 194.22 (C=O), 191.05 (–C=O, aldehyde), 149.54 (C=C), 152.14, 148.65, 138.12, 130.85, 128.76, 127.29, 119.62, 113.81 (Ar–C), 112.80 (C=C), 50.12 (2×CH$_2$), 46.16 (CH$_2$), 40.86 (2×CH$_2$), 39.71 (CH), 31.85 (2×C(CH$_3$)$_2$), 29.09 (CH$_2$), 28.03 (4×CH$_3$), 20.07 (CH$_2$), 13.85 (CH$_3$).

9,9′-((Butylazanediyl)bis(1,4-phenylene))bis(3,3,6,6-tetramethyl-3,4,6,7,9,10-hexahydroacridine-1,8(2H,5H)-dione) (**7**): Yellow solid: m.p. 231–233 °C; IR (KBr, cm^{-1}): 3278, 3072, 2956, 2869, 1631, 1612, 1506, 1486, 1222; ^{1}H·NMR (400 MHz, DMSO-d$_6$) δ (ppm): 8.81 (2H, s, NH), 7.12 (4H, d, $J = 8.5$ Hz, Ar–H), 6.73 (4H, d, $J = 8.5$ Hz, Ar–H), 5.03 (2H, s, 2×CH), 3.70 (2H, t, $J = 6.5$ Hz, N–CH$_2$), 2.33 (4H, d, 2×CH$_2$, $J = 18.0$ Hz), 2.21 (4H, d, 2×CH$_2$, $J = 16.3$ Hz), 2.06 (8H, s, 4×CH$_2$), 1.54–1.51 (2H, m, CH$_2$), 1.29–1.24 (2H, m, CH$_2$), 1.09 (12H, s, 4×CH$_3$), 1.00 (12H, s, 4×CH$_3$), 0.88 (3H, t, $J = 5.5$ Hz); ^{13}C·NMR (100 MHz, CDCl$_3$) δ (ppm): 198.68 (C=O), 151.39 (C=C), 147.07, 128.43, 120.26, 119.96 (Ar–C), 115.19 (C=C), 60.42 (4×CH$_2$), 58.50 (CH$_2$), 50.79 (4×CH$_2$), 32.74 (2×CH), 29.43 (4×C(CH$_3$)$_2$), 27.33 (CH$_2$), 21.08 (8×CH$_3$), 18.45 (CH$_2$), 14.14 (CH$_3$).

4-(Butyl(4-(3,3,6,6-tetramethyl-1,8-dioxo-10-phenyl-1,2,3,4,5,6,7,8,9,10-decahydroacridin-9-yl)phenyl)amino)benzaldehyde (**8**): Orange solid; mp: 106–109 °C; [α]$_D^{20}$ = +71.5° (c = 0.033 g/mL, CHCl$_3$); IR (KBr, cm^{-1}): 2956, 2923, 2869, 1718, 1642, 1592, 1508, 1448, 1249; ^{1}H NMR (400 MHz, CDCl$_3$) δ (ppm): 9.74 (1H, s, CHO), 7.66 (2H, d, $J = 8.8$ Hz, Ar–H), 7.38–7.17 (4H, m, Ar–H), 7.12 (1H, d, $J = 5.5$ Hz, Ar–H), 6.96 (2H, d, $J = 8.5$ Hz, Ar–H), 6.88 (2H, d, $J = 8.6$ Hz, Ar–H), 6.70 (2H, d, $J = 8.5$ Hz, Ar–H), 5.49 (1H, s, CH), 3.71 (1H, t, $J = 7.6$ Hz, N–CH$_2$), 3.62 (1H, t, $J = 7.6$ Hz, N–CH$_2$), 2.45 (2H, d, $J = 13.4$ Hz, CH$_2$), 2.38 (2H, d, $J = 16.0$ Hz, CH$_2$), 2.26 (4H, s, 2×CH$_2$), 1.39–1.33 (2H, m, CH$_2$), 1.28–1.24 (2H, m, CH$_2$), 1.14 (6H, s, 2×CH$_3$), 1.11 (6H, s, 2×CH$_3$), 0.94 (3H, t, $J = 6.7$ Hz, CH$_3$); ^{13}C·NMR (100 MHz, CDCl$_3$) δ (ppm): 190.23 (C=O), 189.28 (–C=O, aldehyde), 160.02 (C=C), 145.93, 131.79, 130.16, 129.42, 128.51, 127.59, 127.20, 125.62, 123.84, 120.51, 115.73, 115.15 (Ar–C), 113.25 (C=C), 50.33 (2×CH$_2$), 47.08 (CH$_2$), 46.47 (2×CH$_2$), 43.76 (CH), 31.37 (2×C(CH$_3$)$_2$), 29.75 (CH$_2$), 27.38 (4×CH$_3$), 20.31 (CH$_2$), 13.96 (CH$_3$).

9,9′-((Butylazanediyl)bis(1,4-phenylene))bis(3,3,6,6-tetramethyl-10-phenyl-3,4,6,7,9,10-hexahydroacridine-1,8(2H,5H)-dione) (**9**): Pale yellow solid; mp: 169–171 °C. IR (KBr, cm^{-1}): 3062, 2960, 1689, 1596, 1571, 1494, 1243; ^{1}H NMR (400 MHz, CDCl$_3$) δ (ppm): 7.61 (2H, d, $J = 8.78$ Hz, Ar–H), 7.86 (4H, t, $J = 7.9$ Hz, Ar–H), 7.18 (4H, d, $J = 7.74$ Hz, Ar–H), 7.13 (4H, t, $J = 7.4$ Hz,

Fig. 1 The X-ray diffraction pattern of TPA NPs/PAA, standard pattern of (TPA), and polymer
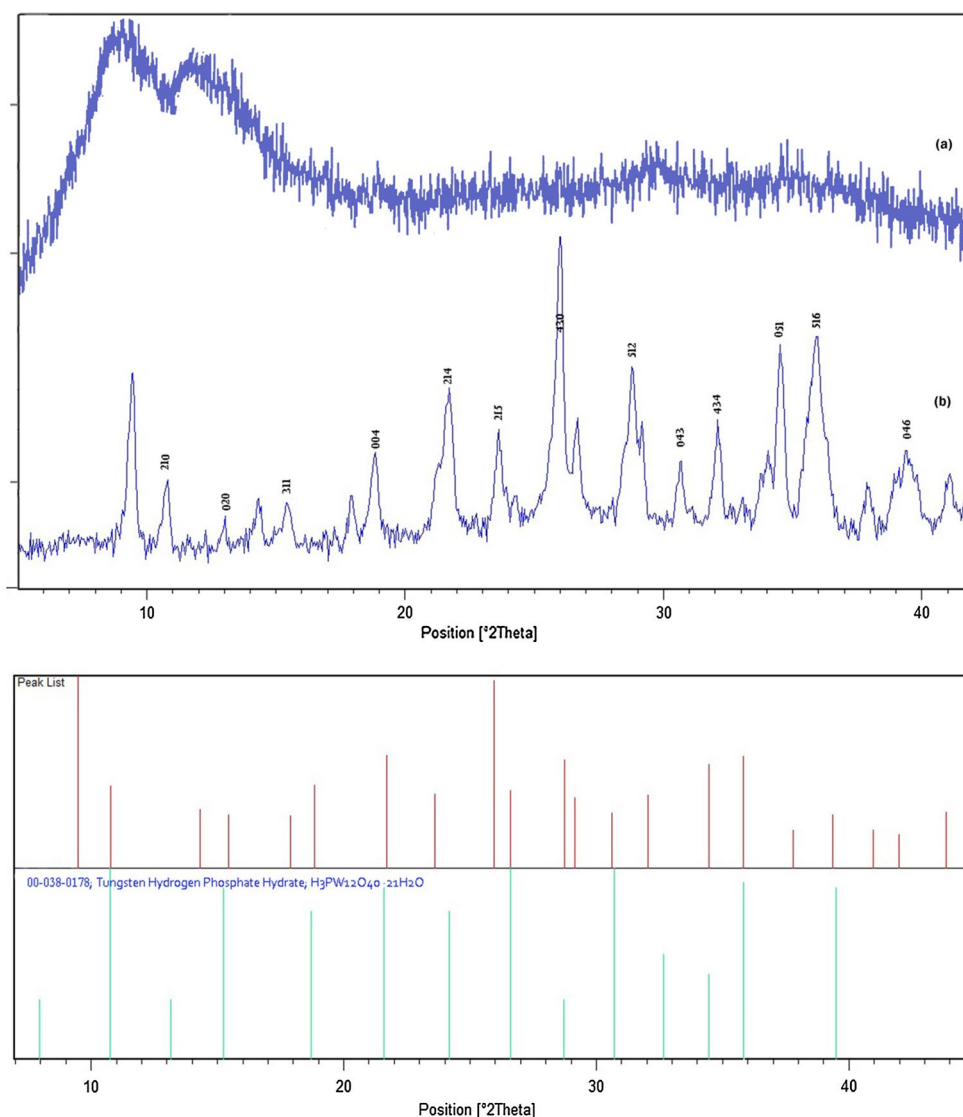
Ar–H), 6.68–6.64 (4H, m, Ar–H), 5.31 (2H, s, CH), 3.69 (2H, t, $J = 7.7$ Hz, N–CH$_2$), 2.38 (8H, s, 4×CH$_2$), 2.05 (8H, s, 4×CH$_2$), 1.32–1.18 (4H, m, 2×CH$_2$), 1.03 (24H, s, 8×CH$_3$), 0.87 (3H, t, $J = 7.7$ Hz, CH$_3$), ^{13}C NMR (100 MHz, CDCl$_3$) δ (ppm): 195.36 (C=O), 160.01 (C=C), 139.14, 139.04, 129.17, 124.29, 122.92, 122.87, 122.80, 122.75 (Ar–C), 110.73 (–C=C), 50.12 (4×CH$_2$), 41.99 (CH$_2$), 41.93 (CH$_2$), 32.25 (4×CH$_2$), 29.55 (4×C(CH$_3$)$_2$), 29.09 (CH$_2$), 28.03 (8×CH$_3$), 27.92 (2×CH), 20.07 (CH$_2$), 13.85 (CH$_3$).

Results and discussion

Characterization of the catalyst

Nanoparticles of tungstophosphoric acid supported on polyamic acid (TPA NPs/PAA) were prepared as a new

heterogeneous catalyst. Figure 1 shows the XRD patterns of the pure polymer (a) and prepared catalyst (b). As seen in Fig. 1, the peak signals at (210), (020), (311), (004), (214), (215), (430), (512), (043), (434), (051), (516), and (046) confirmed the formation of the orthorhombic crystal system, which coincides with the JCPD 038-0178 standard. The size of TPA NPs/PAA powder was also determined by X-ray line broad using the Debye–Scherrer formula given as $D = 0.9\lambda/\beta\cos\theta$, where D is the average crystalline size, λ the X-ray wavelength used (1.5406 Å for Cu Kα), β is the angular line width at half maximum intensity, and θ is the Bragg's angle. The average size of tungstophosphoric acid supported on polyamic acid powder for $2\theta = 9.4679°$ was estimated around 35 nm.

To investigate the morphology and particle size of tungstophosphoric acid supported on polyamic acid, FE-SEM images of TPA NPs/PAA are presented in Fig. 2. This result shows that nanoparticles were obtained with an

Fig. 2 FE-SEM images of the catalyst (TPA NPs/PAA)
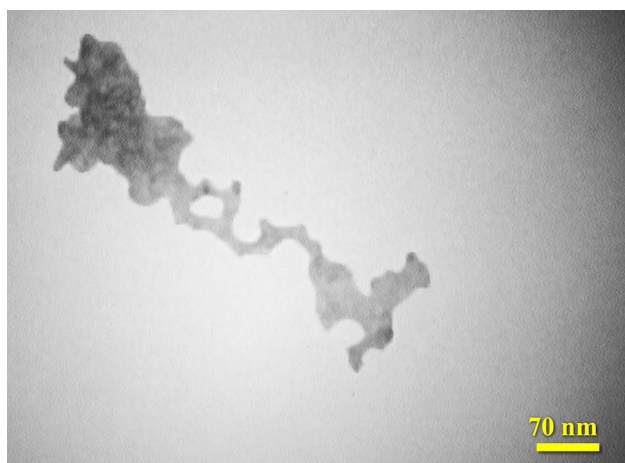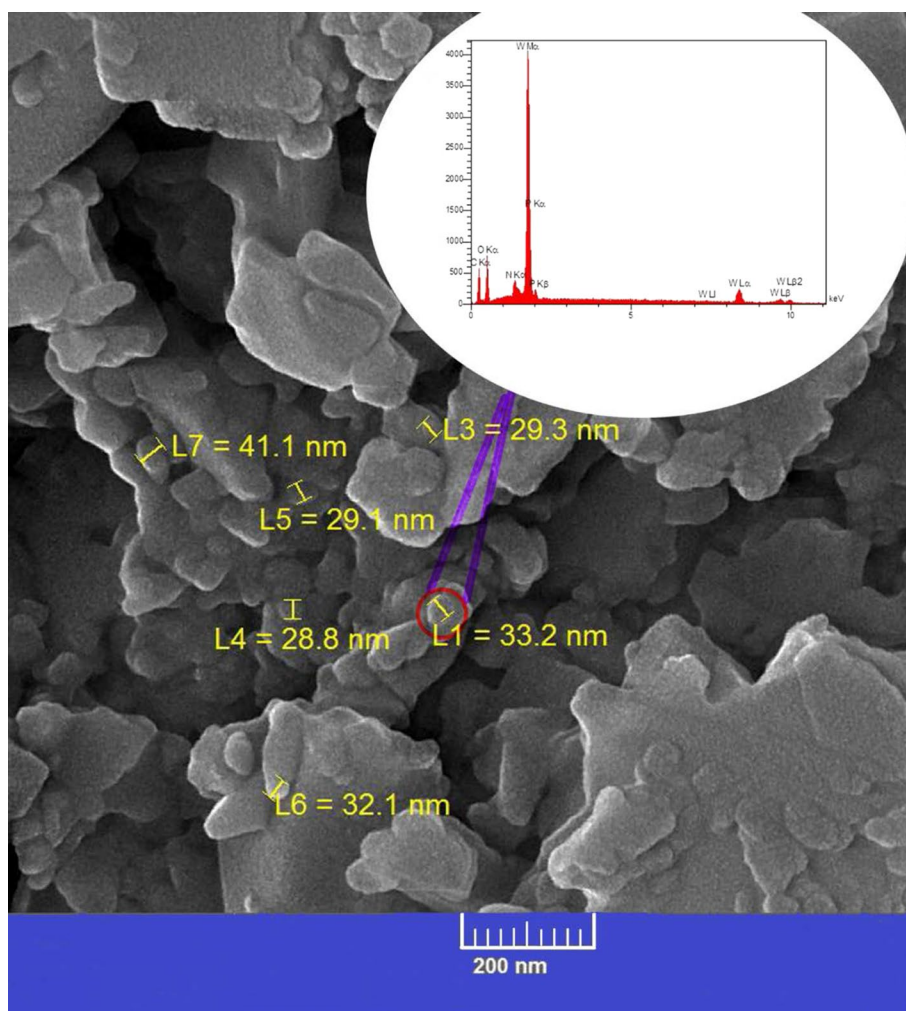

Fig. 3 Transmission electron microscopy (TEM) image of TPA/PAA

average diameter of 40 nm as confirmed by XRD analysis. The transmission electron microscopy (TEM) image of TPA NPs/PAA demonstrated a homogeneous nanostructure and confirmed them to be in nanoscale size, where the dark areas represent the TPA NPs and the gray/white areas the PAA matrix (Fig. 3). The relatively strong interactions between the PAA matrix and TPA NPs were responsible for observing NPs with almost spherical shapes. The NPs size ranged from 15 to 20 nm, except for a very few agglomerates showing a rather spherical shape. The transmission electron microscopy (TEM) image of the TPA NPs/PAA was in good agreement with SEM and XRD analysis and successfully confirmed the supporting of heteropoly acid nanoparticles on the polymer (Fig. 3).

As a useful technique, FT-IR can be used for the study of surface interactions between HPA and organic compounds. Figure 4 shows the FT-IR spectra of pure PAA, TPA, and TPA/PAA. The FT-IR spectrum of the 30 % w/w of TPA on PAA shows four bands in the range 1065 to 634 cm^{-1} related to Keggin bands of heteropoly acid in TPA/PAA (Fig. 4c). However, small shifts of $\nu W = O_d$ (980 cm^{-1}) and $\nu W–O_c–W$ (634 cm^{-1}) vibrations were registered indicating interactions of the support with the most external atoms O_d and O_c of the Keggin anion.

Energy-dispersive X-ray spectroscopy (EDAX) showed the presence of C, N, O, P, and W in tungstophosphoric acid nanoparticles supported on polyamic acid (Fig. 5). The elemental distribution mapping of this analysis shows
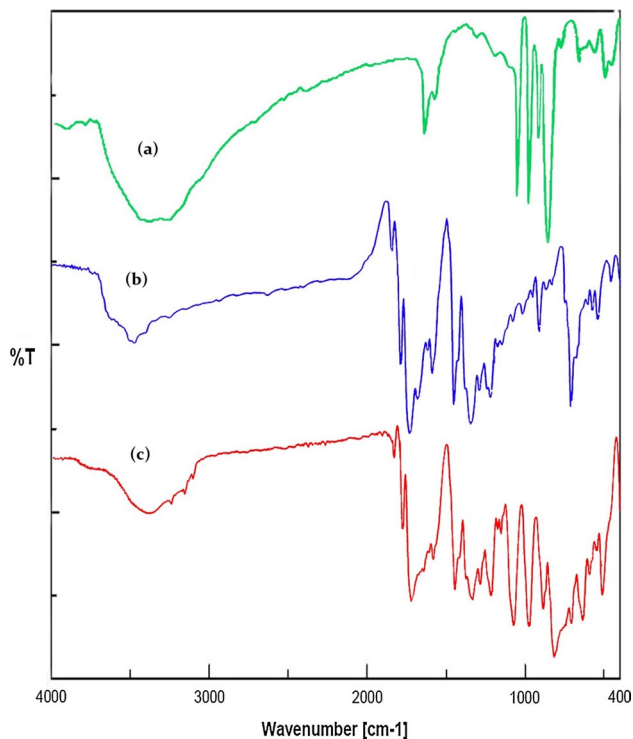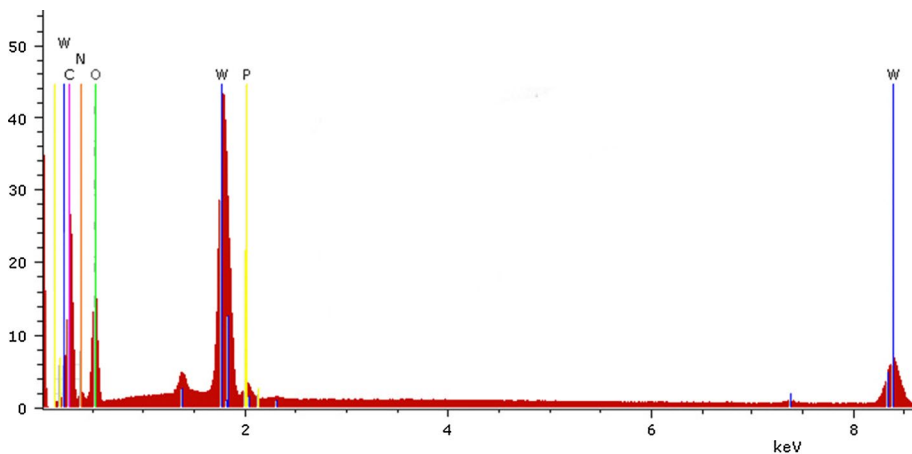

Fig. 4 FT-IR spectra of TPA (*a*), PAA (*b*), and TPA/PAA (*c*)

signals of carbon:nitrogen:oxygen:phosphorous:tungsten in the ratio of 31.7:4.9:16.6:0.7:46.0 wt%, respectively. This confirms the successful incorporation of the expected elements in the material network.

The percentage of tungsten (W) in the catalyst was also determined by ICP-OES analysis which showed 33.6 %w/w of tungsten.

Since the catalyst at different temperatures to be used should also be investigated thermal resistance. For this purpose, the thermogravimetric analyzer (TGA) was used. We observed that the TPA/PAA (Fig. 6) and polyamic acid [32] remained unchanged until 300 °C, but around 40 % decomposed at higher temperatures up to 600 °C. The mass remaining above 600 °C is attributed to the weight percentage of polymer left undecomposed under nitrogen atmosphere [32]. From these data, it is clear that no change in the thermal stability of the polymer occurred on supporting tungstophosphoric acid on polyamic acid [32]. The TG diagram also shows that the supported PAA is decomposed slower than free PAA [32], so that its main decomposition initiates at higher temperature (about 50 °C). This means that TPA enhances the thermal stability of the supported PAA. Moreover, some activation parameters of decomposition thermal steps were evaluated based on the Coats–Redfern model [33] and the results have been compiled in Table 1. Relatively high values of activation energy of decomposition steps confirm the stability of the catalyst. The positive values of enthalpy change and Gibbs free energy indicate the endothermic character of the processes. The negative values of entropy change suggest the

Fig. 5 Energy-dispersive spectroscopy (EDAX) pattern of TPA/PAA

Element	Series	[wt. %]	[Norm. at. %]
Carbon	K-series	31.7417026	61.39100601
Nitrogen	K-series	4.89175618	8.113022304
Oxygen	K-series	16.6157551	24.12515192
Phosphorus	K-series	0.74346449	0.557596412
Tungsten	L-series	46.0073217	5.813223355
	Sum:	100	100

Fig. 6 Thermal gravimetric analysis curves of TPA/PAA
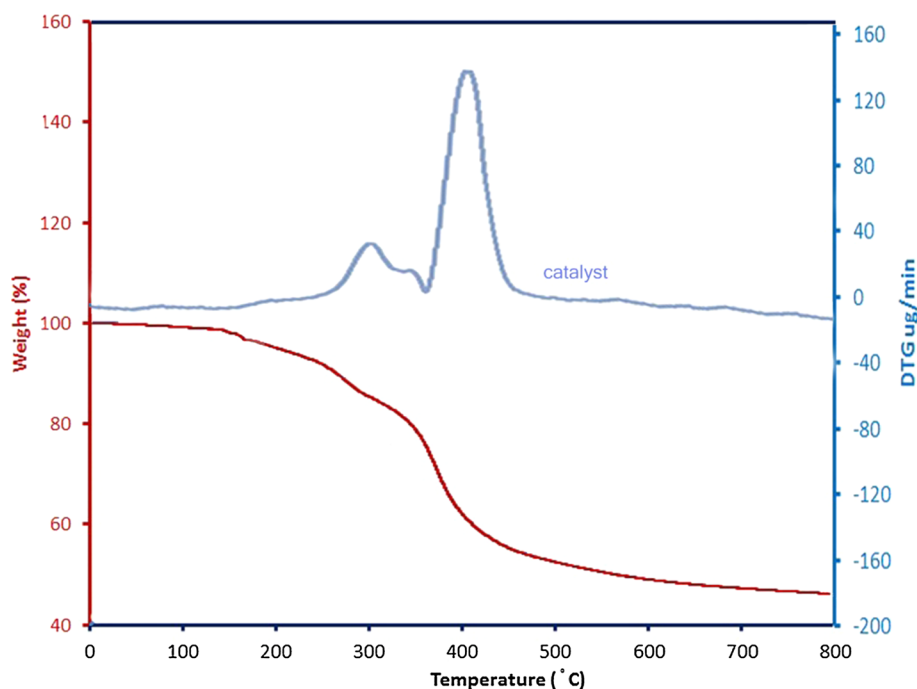
Table 1 Thermal analysis data including temperature range, differential thermogravimetry (DTG) peak, mass loss, and thermokinetic parameters of the thermal decomposition process

Compound	Temp. range (°C)	Mass loss (%)	Peak temp. (°C)	E* (kJ/mol)	A* (1/S)	ΔS* (kJ/mol)	ΔH* (kJ/mol)	ΔG* (kJ/mol)
TPA/PAA	160–240	8.71	198.21	99.3736	2.03×10^8	-8.97×10^1	95.4548	1.38×10^2
	240–346	12.5	277.42	37.4135	4.30	-2.38×10^2	32.8360	1.64×10^2
	346–500	37	405.56	76.1098	2.31×10^3	-1.87×10^2	70.4670	1.98×10^2

abnormal nature of the decomposition process of the current catalyst.

Based on the functional groups in the polymer structure (NH, C=O) and TPA (OH, P=O), it seems that hydrogen bonding and some other polar forces are the most interactive between PAA and TPA [34].

Effect of solvent and catalyst concentration on the synthesis of 1,8-dioxo-decahydroacridines

To evaluate the catalytic activity of TPA NPs/PAA, the reaction of 5,5-dimethyl-1,3-cyclohexanedione (dimedone) (**1**), benzaldehyde (**2a**), and ammonium acetate was carried out as a model reaction. Various reaction parameters such as solvent, catalyst loading, and the molar ratio of reactants were optimized.

For comparison of the results in a solvent and solvent-free conditions, the condensation of ammonium acetate (1 mmol), benzaldehyde (1 mmol), and dimedone (2 mmol) was studied in the presence of TPA NPs/PAA (0.04 g of 30 % w/w tungstophosphoric acid supported on polymer) as a model reaction. As shown in Table 2, among the selected solvents, such as water, ethanol, chloroform, acetonitrile, methanol, toluene, ethanol–water, and a solvent-free system, the best result was obtained after 40 min in ethanol–water (v/v = 1) as a solvent under reflux conditions in excellent yield (Table 2, entry 8).

For investigation of the effect of various amounts of TPA loading on PAA in the synthesis of 1,8-dioxo-decahydroacridines, different weight percents of heteropoly acid were used. Table 2 and Fig. 7a show the differences in the catalytic activity among 10–40 wt% catalysts loading of TPA on PAA. Increment in the loading of the supported tungstophosphoric acid from 10 to 30 wt% causes the acceleration of the reaction rate. Also, no increment in the catalytic activity was observed by increasing the amount of acid on PAA from 30 to 40 wt%. Since 30 wt% of TPA was the best catalyst loading, it was used to study the effect of various parameters on yields. For polyamic acid alone, no noticeable catalytic activity was observed (Table 2, entry 14).

The catalyst concentration was also investigated in the range of 0.01–0.05 g from 30 wt% of the catalyst. The yields of the corresponding 1,8-dioxo-decahydroacridines

Table 2 Optimization of the model reaction[a]

Entry	(Wt%) Catalyst (g)	Temp. (°C)	Solvent[c]	Time (Min)	Yield[b] (%)
1	(30 %) TPA/PAA (0.04)	100	–	60	70
2	(30 %) TPA/PAA (0.04)	Reflux	H_2O	60	85
3	(30 %) TPA/PAA (0.04)	Reflux	C_2H_5OH	60	85
4	(30 %) TPA/PAA (0.04)	Reflux	CH_3CN	60	75
5	(30 %) TPA/PAA (0.04)	Reflux	CH_3OH	60	80
6	(30 %) TPA/PAA (0.04)	Reflux	$CHCl_3$	60	50
7	(30 %) TPA/PAA (0.04)	Reflux	Toluene	60	75
8	(30 %) TPA/PAA (0.04)	Reflux	C_2H_5OH/H_2O	40	92
9	(30 %) TPA/PAA (0.03)	Reflux	C_2H_5OH/H_2O	40	85
10	(30 %) TPA/PAA (0.05)	Reflux	C_2H_5OH/H_2O	40	92
11	(20 %) TPA/PAA (0.04)	Reflux	C_2H_5OH/H_2O	40	70
12	(40 %) TPA/PAA (0.04)	Reflux	C_2H_5OH/H_2O	45	90
13	TPA (0.012)	Reflux	C_2H_5OH/H_2O	40	70
14	PAA	Reflux	C_2H_5OH/H_2O	60	Trace
15	–	Reflux	C_2H_5OH/H_2O	60	Trace

[a] Reaction condition: dimedone (2 mmol), benzaldehyde (1 mmol), and ammonium acetate (1 mmol)
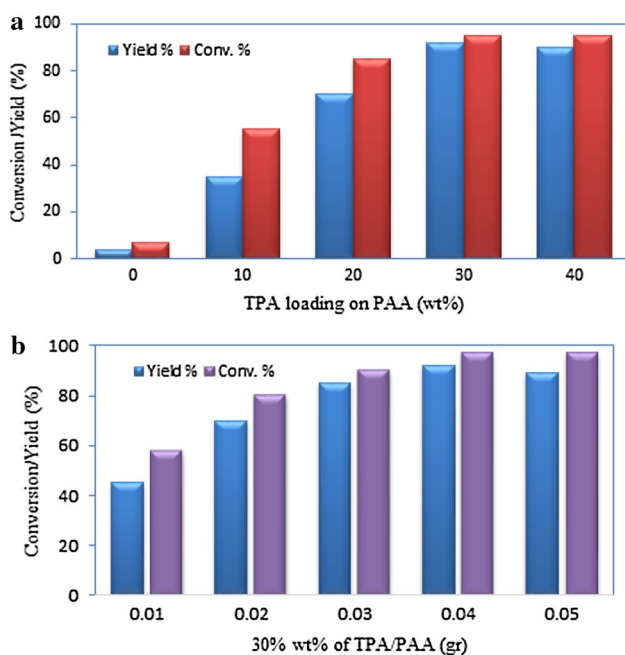
[b] Isolated yields

[c] 2 mL of solvent(s) (v/v = 1)

Fig. 7 Catalytic activities of nanoparticles $H_3PW_{12}O_{40}$/polyamic acid in the synthesis of **3a**: **a** conversions and yields against different loading of catalyst on the polymer, **b** conversions and yields for different amounts of 30 wt% of the catalyst

were increased with increasing catalyst concentration from 0.0072 to 0.0096 mmol of H^+ (0.03–0.04 g, Fig. 7b). Further addition of catalyst had no noticeable effect on the yield, because there exist an excess of catalyst sites over what is actually required by the reactant molecules

(Fig. 7b). Therefore, in further reactions 0.0092 mmol of H^+ (equal to 0.32 mol% of TPA) was used for 30 wt% of tungstophosphoric acid (Table 2, entry 8).
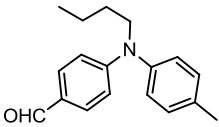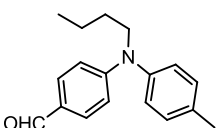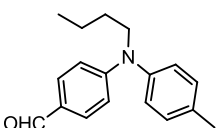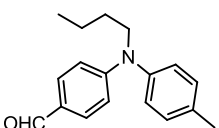
Hence, performing the reaction in refluxing ethanol–water and in the presence of 0.04 g of 30 wt% of catalyst was determined as the optimal condition. Using the optimized reaction conditions, the scope and limitations of this protocol were evaluated using a variety of aromatic aldehydes (Table 3).

Surprisingly, it was observed that both mono- and bis-1,8-dioxo-decahydroacridines can be selectively obtained by this catalytic system. As shown in Table 3, mono- and bis-1,8-dioxo-decahydroacridines were produced from dialdehydes **5** (as bulky molecules) in 70–80 % yields with appropriate reaction times (50–60 min). The preparation of mono-dioxo-decahydroacridines from dialdehydes is of great interest, because the remaining formyl group can be converted to other useful functional groups.

A substituted amine with three different ligands is chiral, but racemization via pyramidal N-inversion is often too fast for separation of enantiomers at room temperature. In general, the barrier energy of nitrogen inversion decreases as the bulkiness of the substituents increases because of destabilizing steric repulsion in the pyramidal ground state. Inversion at the sp^3-hybridized nitrogen occurs via a planar transition state. An increase in the p-character of the nitrogen bonds, therefore, prevents N-inversion [43].

Due to these scientific principles, the optical rotations of **6** and **8** as bulky chiral amines were investigated and the change in the orientation of monochromatic plane-polarized light (+109.2° and +71.5° specific rotations using

Table 3 Synthesis of 1,8-dioxo-decahydroacridines and bis (1,8-dioxo-decahydroacridine) catalyzed by nanoparticles TPA/PAA[a]

Entry	Ar	Amine	Product	Time (min)	Yield (%)[b]	Mp (°C)[c]	Ref.
1	C_6H_5	NH_4OAc	**3a**	40	92	290–291	[35]
2	$3\text{-}NO_2C_6H_4$	NH_4OAc	**3b**	30	95	307–308	[36]
3	$4\text{-}NO_2C_6H_4$	NH_4OAc	**3c**	28	96	284–286	[37]
4	$4\text{-}CH_3C_6H_4$	NH_4OAc	**3d**	45	85	278–280	[38]
5	$4\text{-}ClC_6H_4$	NH_4OAc	**3e**	33	90	298–300	[39]
6	$4\text{-}BrC_6H_4$	NH_4OAc	**3f**	35	92	308–310	[40]
7	$4\text{-}CH_3OC_6H_4$	NH_4OAc	**3g**	50	80	276–278	[41]
8	C_6H_5	Aniline	**4a**	38	90	253–255	[42]
9	$3\text{-}NO_2C_6H_4$	Aniline	**4b**	30	97	298–300	[13]
10	$4\text{-}NO_2C_6H_4$	Aniline	**4c**	25	95	288–290	[16]
11	$4\text{-}CH_3C_6H_4$	Aniline	**4d**	45	88	260–262	[16]
12	$4\text{-}ClC_6H_4$	Aniline	**4e**	30	90	244–246	[13]
13	$4\text{-}BrC_6H_4$	Aniline	**4f**	35	95	254–256	[16]
14	$4\text{-}CH_3OC_6H_4$	Aniline	**4 g**	48	82	219–221	[13]
15		NH_4OAc	**6**	53	70	161–163	–
16		Aniline	**8**	55	75	106–109	–
17		NH_4OAc^d	**7**	60	73	231–233	–
18		Aniline[d]	**9**	50	80	169–171	–

[a] Reaction conditions: dimedone (2 mmol), aldehyde (1 mmol), amine (1 mmol), catalyst (0.04 g), solvent (2 mL)

[b] Melting points are uncorrected

[c] Isolated yield

[d] Dimedone (4 mmol), amine (2 mmol, ammonium acetate for **7** and aniline for **9**), and catalyst (0.08 g)

6 and **8** solutions with 0.021 and 0.033 g/mL concentration in $CHCl_3$ as a solvent, respectively) was surprisingly observed. According to the observed optical rotation for the polymer ($[\alpha]_D^{20} = +38.4°$, $c = 0.005$ g/mL in DMF), it seems that this chirality characteristic of the polymer is the main factor for these asymmetric syntheses of the chiral amines.

The dialdehyde **5** was synthesized using the Vilsmeier reaction according to the literature (Scheme 4) [44]. 1-Bromobutane was reacted with diphenylamine in the presence of sodium hydroxide in DMSO to give *N*-butyl-*N*-phenylaniline. Under a nitrogen atmosphere, $POCl_3$ was added to DMF, then the amine was added to this solution, and the resulting mixture was stirred. After cooling and basifying with sodium hydroxide solution, the resulting mixture was extracted and purified by column chromatography to give 4,4′-(butylazanediyl) dibenzaldehyde (**5**).

Recovery and reusability of the catalyst

From the industrial viewpoint, the recovery and reusability of the catalyst are important for the large-scale operation.
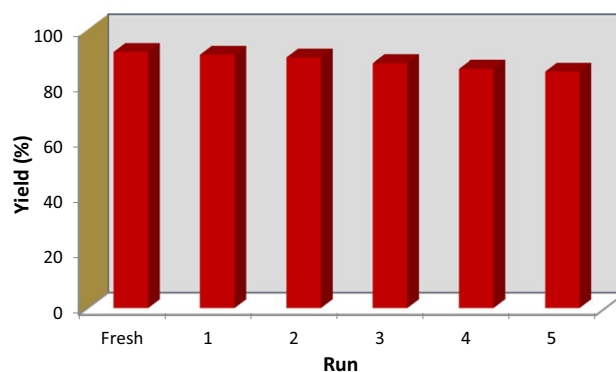

Fig. 8 Recyclability of TPA NPs/PAA in the synthesis of 1,8-dioxo-decahydroacridines

It is noteworthy that the catalyst was recovered simply by filtration without any acidic or basic workup even after its five uses. After completion of the reaction of benzaldehyde, amine, and dimedone, the catalyst was recovered from the reaction mixture and the recovered catalyst was washed with ethanol and dried. By ICP-OES analysis, it was

Fig. 9 FT-IR spectra of *a* fresh TPA/PAA and *b* reused catalyst
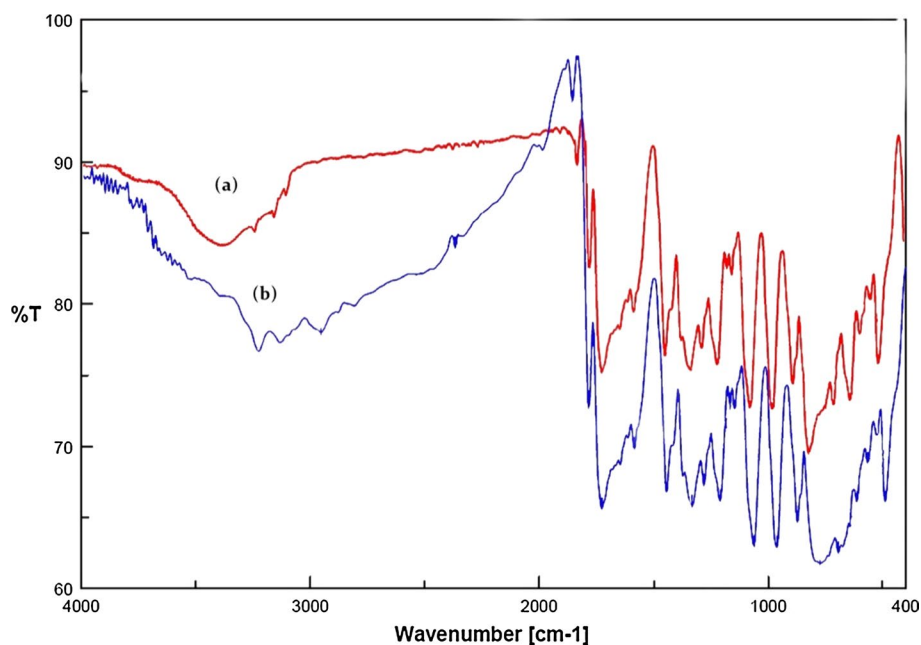
Scheme 5 The proposed mechanism for the TPA/PAA promoted the synthesis of 1,8-dioxo-decahydroacridine
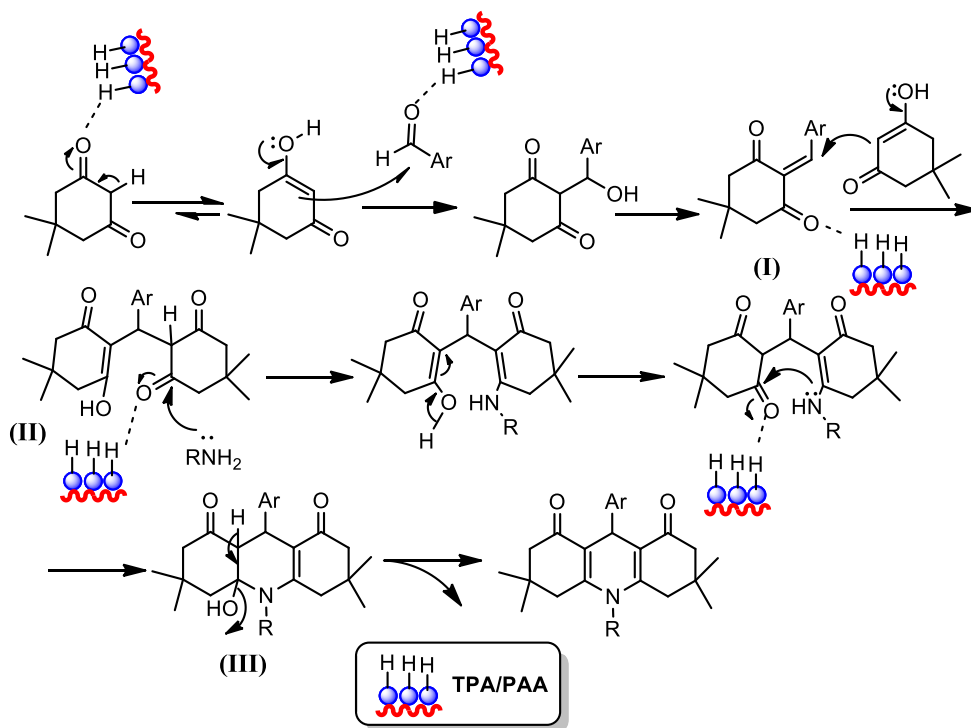
showed that the amount of tungsten present in the filtrate was very low (3.5×10^{-4} %w/w of supported heteropoly acid).

The recovered catalyst was added to fresh substrates under the same experimental conditions for five runs without a noticeable decrease in the product yield and its catalytic activity (Fig. 8). The IR peaks appeared at the catalyst spectrum after the reaction was well in agreement with those obtained for the fresh catalyst, which confirmed that the structure of the catalyst remained unchanged after recycling (Fig. 9).

As TPA/PAA is not soluble in ethanol and water, no catalyst leaching, as well as no contribution of homogeneous catalysis in the course of the reaction, was expected. To rule out the contribution of homogeneous catalysis, the standard leaching experiment was conducted. A model reaction was

Table 4 Comparison of the efficiency of various catalysts in the synthesis of 1,8-dioxo-decahydroacridine

Entry	Catalyst	Conditions	Time (min)	Yield (%)	Ref.
1	Ceric ammonium nitrate	PEG-400/50 °C	210–240	93–98	[13]
2	FSG-Hf(NPf$_2$)$_4$	EtOH/H$_2$O/reflux	180–420	Trace-83	[18]
3	TiO$_2$ NPs	EtOH/reflux	60–100	82–91	[19]
4	Triethylbenzylammonium chloride	H$_2$O/reflux	240–480	90–98	[27–31]
5	[Hmim]TFA	Solvent free/80 °C	240–420	78–89	[45]
6	HY-Zeolite	EtOH/reflux	150–210	70–90	[46]
7	TPA NPs/PAA	EtOH/H$_2$O/reflux	25–60	70–96	–

preceded for 5 min in the presence of the catalyst and then the catalyst was removed by filtration. The reaction was allowed to proceed without a catalyst. There was no change in the progress of the reaction even after 6 h, indicating that no leaching had occurred and therefore, no homogeneous catalyst was involved.

The proposed mechanism in which TPA/PAA has catalyzed this transformation is shown in Scheme 5. The reaction proceeds via one-pot Knoevenagel condensation, Michael addition, enamine formation, and cyclodehydration. The acid catalyst changes the aldehyde into convenient electrophile via activation of the carbonyl group and then one molecule of dimedone condenses with the aldehyde to produce an intermediate (I). Then the second molecule of dimedone reacts with this intermediate to give intermediate II. Nucleophilic attack of the amine group to the carbonyl group is followed by cyclization leading to the formation of intermediate III. Finally, by the removal of one water molecule, acridine derivatives will be obtained.

To show the ability of our method with respect to previous reports, some of our results in comparison to some other methods are summarized in Table 4. As shown, the yield/time ratio of the present method is better or comparable to the other reported results.

Conclusions

In summary, we have described an improved procedure for the selective synthesis of 1,8-dioxo-decahydroacridines and bulky bis(1,8-dioxo-decahydroacridine)s using tungstophosphoric acid nanoparticles supported on polyamic acid (TPA NPs/PAA) as a new, heterogeneous, and recoverable catalyst. The mono- and bis-decahydroacridines as crowded molecules can be obtained by this catalytic system in good to excellent yields. Also, bulky chiral amines are synthesized due to chirality characteristic of the polymer. The mild reaction conditions, rapid conversion, high yields, simple experimental procedure, and recoverability of the catalyst are notable advantages of the present method.

References

1. N.S. Burres, S. Sazesh, G.P. Gunawardana, J.J. Clement, Cancer Res. **49**, 5267 (1989)
2. D. Greenwood, J. Antimicrob. Chemother. **36**, 857 (1995)
3. L. Ngadi, A.M. Galy, J.P. Galy, J. Barbe, A. Cremieux, J. Chevalier, D. Sharples, Eur. J. Med. Chem. **25**, 67 (1990)
4. M. Wainwright, J. Antimicrob. Chemother. **47**, 1 (2001)
5. O. Berkan, B. Sarac, R. Simsek, S. Yildirim, Y. Sariogli, C. Safak, Eur. J. Med. Chem. **37**, 519 (2002)
6. Y. Takemura, M. Ju-ichi, C. Ito, H. Furukawa, H. Tokuda, Planta Med. **61**, 366 (1995)
7. S. Harkishan, V.K. Kapoor, Medicinal and Pharmaceutical Chemistry, 2nd edn. (Vallabh Prakashan, Delhi, 2005) pp. 364–365 and 473–475
8. M.A. Horstmann, W.A. Hassenpflug, U. zur Stadt, G. Escherich, G. Janka, H. Kabisch, Haematologica **90**, 1701 (2005)
9. P. Murugan, P. Shanmugasundaramn, V.T. Ramakrishnan, B. Venkatachalapathy, N. Srividya, P. Ramamurthy, K. Gunasekaran, D. Velmurugan, J. Chem. Soc. Perkin Trans. **2**, 999 (1998)
10. A. Islam, P. Murugan, K.C. Hwang, C.H. Cheng, Synth. Met. **139**, 347 (2003)
11. S.J. Tu, C. Miao, Y. Gao, F. Fang, Q. Zhuang, Y. Feng, D. Shi, Synlett **2**, 255 (2004)
12. B. Das, P. Thirupathi, I. Mahender, V.S. Reddy, Y. Koteswara, J. Mol. Catal. A-Chem. **247**, 233 (2006)
13. M. Kidwai, D. Bhatnagar, Tetrahedron Lett. **51**, 2700 (2010)
14. W. Shen, L.M. Wang, H. Tian, J. Tang, J.J. Yu, J. Fluorine Chem. **130**, 522 (2009)
15. X. Fan, Y. Li, X. Zhang, G. Qu, J. Wang, Heteroat. Chem. **18**, 786 (2007)
16. T.S. Jin, J.S. Zhang, T.T. Guo, A.Q. Wang, T.S. Li, Synthesis **12**, 2001 (2004)
17. A.K. Dutta, P. Gogoi, R. Borah, RSC Adv. **4**, 4128 (2014)
18. M. Hong, G. Xiao, J. Fluorine Chem. **144**, 7 (2012)
19. S.M. Vahdat, S. Khaksar, M. Akbari, S. Baghery, Arabian J. Chem. (2014). doi:10.1016/j.arabjc.2014.10.026
20. H. Alinezhad, M. Tajbakhsh, M. Norouzi, A. Baghery, J. Rakhtshah, J. Chem. Sci. **125**, 1517 (2013)
21. J. Safaei-Ghomi, M.A. Ghasemzadeh, S. Zahedi, J. Mex. Chem. Soc. **57**, 1 (2013)
22. S. Rahmani, A. Amoozadeh, JNS **4**, 91 (2014)
23. G. Mohammadi-Ziarani, S. Mousavi, Iran. J. Chem. Chem. Eng. **32**, 9 (2013)
24. M.A. Ghasemzadeh, J. Safaei-Ghomi, H. Molaei, C. R. Chim. **15**, 969 (2012)

25. E. Rafiee, S. Eavani, M. Khodayari, Chin. J. Catal. **34**, 1513 (2013)
26. R. Fazaeli, H. Aliyan, S. Mallakpour, Z. Rafiee, M. Bordbar, Chin. J. Catal. **32**, 582 (2011)
27. M. Nasr-Esfahani, S.J. Hoseini, F. Mohammadi, Chin. J. Catal. **32**, 1484 (2011)
28. M. Nasr-Esfahani, T. Abdizadeh, J. Nanosci. Nanotechnol. **13**, 5004 (2013)
29. M. Nasr-Esfahani, S.J. Hoseini, M. Montazerozohori, R. Mehrabi, H. Nasrabadi, J. Mol. Cal. A-Chem. **382**, 99 (2014)
30. M. Nasr-Esfahani, M. Taei, RSC Adv. **5**, 44978 (2015)
31. M. Nasr-Esfahani, D. Elhamifar, T. Amadeh, B. Karimi, RSC Adv. **5**, 13087 (2015)
32. H. Sadeghipour, Z. Rafiee, D. Ashouri, A. Ahmadi, S. Mousavian, A. Hekmati, High Perform. Polym. **27**, 31 (2015)
33. A.W. Coats, J.P. Redfern, Nature **201**, 68 (1964)
34. F. Lefebvre, J. Chem. Soc., Chem. Commun. 756 (1992)
35. X.S. Wang, M.M. Zhang, H. Jiang, D.Q. Shi, S.J. Tu, X.Y. Wei, Z.M. Zong, Synthesis 4187 (2006)
36. G.W. Wang, J.J. Xia, C.B. Miao, X.L. Wu, Bull. Chem. Soc. Jpn **79**, 454 (2006)
37. M.J. Wainwright, Antimicrob. Chemother. **47**, 1 (2001)
38. X. Fan, Y. Li, X. Zhang, G. Qu, J. Wang, Heteroat. Chem. **18**, 786 (2007)
39. A.A. Bakibaev, V.D. Fillimonov, E.S. Nevgodova, Zh Org, Khim. **27**, 1519 (1991)
40. A. Dömling, I. Ugi, Angew. Chem, Int. Ed. 39, 3168 (2000)
41. N. Martin, M. Quinteiro, C. Seoane, J.L. Soto, A. Mora, M. Suárez, A. Morales, E. Ochoa, J.D. Bosque, J. Heterocycl. Chem. **32**, 235 (1995)
42. B. Das, P. Thirupathi, I. Mahender, V.S. Reddy, Y.K. Rao, J. Mol. Catal. A-Chem. **247**, 233 (2006)
43. C. Wolf, Dynamic stereochemistry of chiral compounds: principles and applications, (RSC Publishing, 2008), Chapter 3, pp. 29–135
44. D.J. Kim, S.H. Kim, T. Zyung, J.J. Kim, I. Cho, S.K. Choi, Macromolecules **29**, 3657 (1996)
45. M. Dabiri, M. Baghbanzadeh, E. Arzroomchilar, Cata. Commun. **9**, 939 (2008)
46. M. Nikpassand, M. Mamaghani, K. Tabatabaeian, Molecules **14**, 1468 (2009)